Reduction of Raman Scattering in a Plasma to Convective Levels Using Induced Spatial Incoherence

S. P. Obenschain, C. J. Pawley, A. N. Mostovych, J. A. Stamper, J. H. Gardner, A. J. Schmitt, and S. E. Bodner

U.S. Naval Research Laboratory, Washington, D.C. 20375

(Received 24 October 1988)

We present measurements of the Raman backscatter produced by laser-plasma interaction where the laser focal profile was smoothed by induced spatial incoherence (ISI). The Raman backscatter with the ISI beam is much smaller than that with an ordinary beam. The onset of Raman backscattering with ISI followed the predictions of a convective gain model to within 30% in intensity.

PACS numbers: 52.40.Nk, 52.50.Lp

The Raman instability in a laser-irradiated plasma involves the decay of the incident electromagnetic wave into an electron plasma wave and a scattered electromagnetic wave. Theory predicts that for laser light incident on a monotonically increasing plasma profile, the instability should be absolute for plasma densities near quarter critical density ($n = n_c/4$) and should grow convectively for $n < n_c/4$.[1] The Raman instability is potentially deleterious to laser fusion because the excited electron plasma waves can accelerate electrons and produce unacceptable preheat of the pellet.

Numerous experiments have studied the interaction of lasers with targets for the regime $n < n_c/4$ where the instability should be convective.[2–7] Over a broad range of intensities and laser wavelengths (1060–260 nm), a similar result has been obtained: The Raman scattering occurred at anomalously low intensities compared to the predictions for convective growth of the instability. Several mechanisms have been proposed for this phenomenon including the following: (a) Hot spots in the incident laser beam undergo filamentation and the resulting higher intensity enhances the Raman gain; (b) temporal modulations in the plasma density profile produce flat density regions that enhance the Raman gain; (c) density cavities or mode coupling causes the instability to become absolute[8]; (d) the observed scattering is Thomson scattering rather than Raman.[9] Up to now, the only practical means to control the instability involved use of the combination of short laser wavelength and high-Z (high-atomic-number) targets to provide collisional damping.[6] In this paper we present the very different results obtained using an induced spatial coherence (ISI) smoothed laser beam. Here we demonstrate control of the instability despite the use of low-Z targets and a relatively long (1054 nm) laser wavelength.

ISI is an optical technique for obtaining the highly uniform target illumination required for high-gain laser fusion.[10,11] With ISI, a broadband laser beam is divided into numerous independent beamlets by transmitting or reflecting echelons. The echelons impose time delays between the beamlets where the incremental delays are longer than the laser coherence time $\tau_c = 1/\Delta\nu$. The beamlets are then overlapped onto the target with a lens. The overlapped beamlets form a time-varying interference pattern which converges on a smooth focal profile if one averages over a time period that is long compared to τ_c. Some high-power lasers suitable for laser fusion have sufficient bandwidths to achieve τ_c as short as 1 psec. This should be short enough so that targets irradiated with multinanosecond pulses will react hydrodynamically as if the ISI profile is very smooth. However, fast-growing instabilities, such as the Raman instability, can be influenced by the instantaneous nonuniformity with ISI.

Figure 1 shows the experimental arrangement. We used two beams of the NRL Pharos III Nd-glass laser facility, one with and one without ISI echelons. Both beams are plane polarized and have a 2-nsec FWHM pulse duration. Echelons break the 20-cm-diam ISI beam into about 350 beamlets, each 0.95 cm×0.75 cm. The echelons provide a minimum of a 2-psec differential delay between beamlets. The echelons stretch the duration of the ISI beam by approximately 700 psec. Both beams are focused onto 200-μm-thick by 2-mm-wide plastic (CH) targets using 2.2-m focal-length lenses.

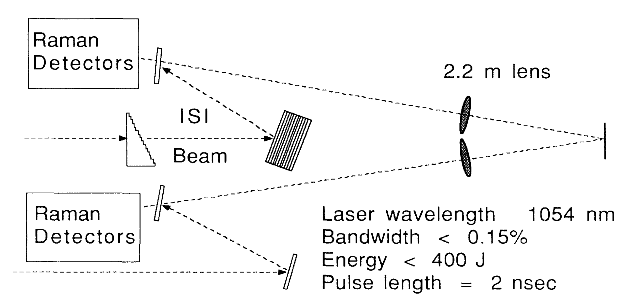

FIG. 1. Experimental arrangement for the study of the effects of ISI on the Raman instability. The Raman detectors are located behind the final turning mirrors before the target. These dielectric-coated-glass mirrors are highly reflective at 1054 nm, but pass the 1300–2200-nm Raman-band emission.

The angle between the beams is 8° and the target normal is midway between the two beams. The coherence time of the laser was varied from $\tau_c = 2$ nsec (the time-bandwidth limit) to $\tau_c = 2$ psec. The envelope of the laser pulse was monitored by silicon diodes with a 0.4-nsec response that averaged over the picosecond temporal structure of the broadband pulses. The time-averaged intensities referred to later in the paper are determined by these diodes. Spectrally filtered detector arrays monitored the Raman backscatter passing back through each focusing lens.

We studied the effects of the ISI echelons and the laser bandwidth on Raman backscatter. In the first set of measurements to be presented here, we alternated between the two laser beams. With broadband ISI, we obtained a time-averaged smooth focal profile similar to the $\text{sinc} = \sin^2(x)/x^2$ function predicted theoretically, but with a FWHM typically 10% larger than predicted due to imperfections in the beamlets and beamlet overlap. The ordinary laser beam had a top-hat-shaped focal profile with intensity structure across the top due to beam imperfections. The diameter (350 μm) of the flat portion of the focus was adjusted to be slightly larger than the 300-μm FWHM focal diameter of the ISI beam, so that the average intensity across the top matched the average intensity across the FWHM diameter of the ISI beam at a given laser energy. The average intensity for both was approximately 10^{14} W/cm^2 for $E = 300$ J. The ordinary beam's focal profile had intensity hot spots that extended a factor of 2–3 above the average. The bandwidth variations employed here had no measurable effect on the focal distribution without ISI. With narrow-band ISI, the beamlet interference pattern is frozen and one obtains a stationary focal profile similar to that obtained instantaneously with broadband ISI.

Figure 2 shows the peak Raman backscatter in the 1350–1750-nm band $[(1.3\text{–}1.7)\lambda_0]$ for the case of broadband ISI ($\tau_c = 2$ psec), narrow-band ISI, and the ordinary beam with narrow bandwidth. The intensity was varied by varying the laser energy. The data were obtained using germanium detectors that have a 0.6-nsec time resolution. The Raman emission with the ordinary beam and the narrow-band ISI beam is orders of magnitude higher than that obtained with broadband ISI. Variations in bandwidth had little effect on the Raman emission with the ordinary laser beam. On the other hand, we observed a strong bandwidth effect with the ISI echelons; the Raman backscatter was suppressed for coherence times shorter than 10 psec. The inset of Fig. 2 shows Raman-backscatter signals obtained using the ISI beam with narrow and with broad bandwidth, both with laser energy near 180 J. The backscatter signal with narrow-band ISI is somewhat shorter than the laser pulse, while the signal with ISI is of much longer duration than the laser pulse, indicating that the backscatter emission is dominated by thermal radiation from the laser-heated target.

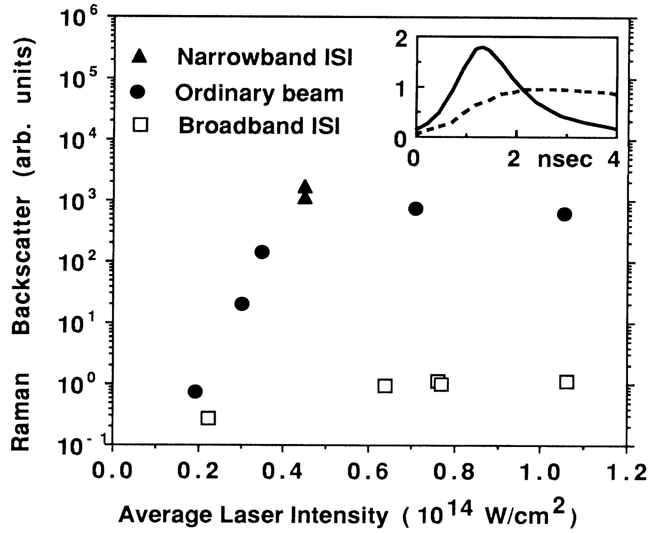

FIG. 2. The peak Raman backscatter in the band 1350–1750 nm for the case of broadband ISI, narrow-band ISI, and an ordinary laser beam with narrow bandwidth. The intensities against which the data are plotted are the averages across the FWHM of the ISI focal distribution, and the average across the "flat top" portion of the ordinary beam. Inset: Typical pulse shapes of the Raman emission obtained with narrow-band ISI (solid line) and broadband ISI (dashed line) with spatially averaged intensities of 5×10^{13} and 6×10^{13} W/cm^2, respectively. The amplitude of the narrow-band pulse is multiplied by a factor of 10^{-3}.

Calibrated detectors (accurate to within $\pm 30\%$) indicated that the peak backscatter emission near $1.53\lambda_0$ (at 0°) and near $1.73\lambda_0$ (at 8°) was near that expected for a thermal source when utilizing broadband ISI at intensities below the experimental threshold (see Fig. 3 for the $1.53\lambda_0$ data). The peak emission at $1.53\lambda_0$ and $1.73\lambda_0$ was 5 to 7 times that calculated for a blackbody with the underdense-plasma coronal temperature (1100–1330 eV from a hydrocode simulation) and an area equal to the (FWHM)^2 of the ISI beam. The targets employed in this experiment had lateral dimensions large compared to the laser beam FWHM and it is believed that the excess emission is originating from hot plasma outside the FWHM of the beam. In a similar experiment using a 527-nm laser, the peripheral emission was reduced by using a small-diameter disk target. With broadband ISI, the peak target emission in the convective Raman band was then observed to be 60%–80% of that for an ideal blackbody. Thus it is believed that the noise source from which the Raman backscatter would grow with broadband ISI is thermal emission.

Broadband ISI provides some mechanism for reducing the Raman backscatter that was observed with the other two focal conditions. As discussed below, the laser bandwidth is probably too small to allow the beam smoothing to directly suppress Raman backscatter. Since we observed suppression of Raman backscatter with τ_c as long as 10 psec, the suppression must involve phenomena that occur on a relatively long time scale, such as density profile fluctuations or filamentation. Computer simulations indicate that, under our experimental conditions, the stationary intensity modulations with either narrowband ISI or the ordinary laser beam are susceptible to strong ponderomotive filamentation, while the broadband ISI beam is resistant to filamentation.[12] The suppression of Raman backscatter by stimulated Brillouin scattering (SBS) that has been observed in other experiments[13] could not occur here because SBS was also suppressed by broadband ISI.[14]

We were able to obtain larger Raman signals with the broadband ISI beam by focusing it onto a preplasma produced by the ordinary laser beam. The focal diameter of the ordinary beam was increased to 1 mm for these experiments to produce a larger plasma, and to maintain a low enough intensity to prevent the preplasma beam from also exciting the Raman instability. The peak of the 350-J preplasma beam preceded the peak of the ISI beam by 2 nsec. Figure 3 shows the Raman emission near 1610 nm (± 40-nm range) with the ISI beam, with and without the preplasma. The data are plotted as a function of the laser intensity at the peak of the sinc^2 focal distribution of the ISI beam. The presence of the preplasma increases the Raman-band emission with ISI, presumably due to a longer-scale-length plasma. The

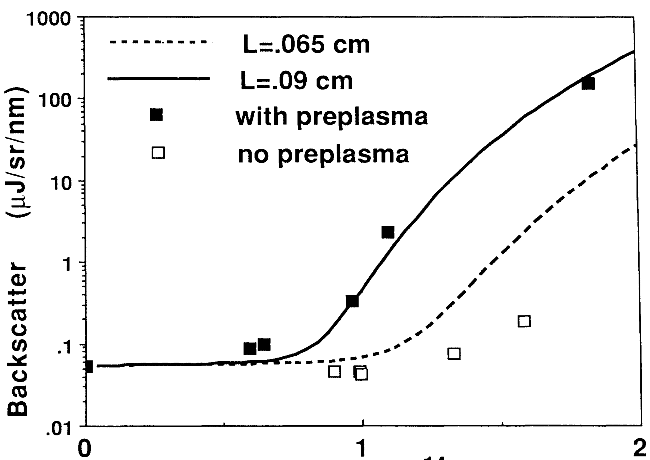

FIG. 3. Raman backscatter near $1.53\lambda_0$ with broadband ISI, but with and without a preplasma. The data are plotted as a function of the time-averaged intensity I_0 at the peak of the sinc^2 focal distribution. This intensity is 1.4 times larger than the spatially averaged intensities used to plot the data in Fig. 2. The data were obtained using calibrated indium-arsenide detectors that time integrated the emission obtained during the entire laser pulse. The theoretical curves are calculated with Eq. (1). The data without the preplasma extend to somewhat higher laser intensity than that in Fig. 2, and some measurable Raman backscatter appears above the background emission.

wave-number and frequency matching conditions for Raman backscatter indicates that the backscatter near 1610 nm ($1.53\lambda_0$) originated near $n=0.1n_c$. The axial density-gradient scale length $L=n/(\delta n/\delta z)$ with only the preplasma beam was measured with interferometry to be 0.06 cm at $0.1n_c$ at the time when the peak of the ISI pulse reaches the target. Two-dimensional hydrocode calculations indicate that the ISI beam at the highest intensities used here heats the underdense preplasma from 600 to 1200 eV, but the axial density scale length near $0.1n_c$ remains nearly constant as the ISI beam intensity is varied. The code gives density scale lengths ranging from 0.064 cm without the ISI beam to 0.067 cm with the ISI beam at 1.4×10^{14} W/cm^2. Both interferometry and the hydrocode give L a factor of 2 shorter with the ISI beam alone.

The theoretical expression for convective Raman backscatter in an inhomogeneous plasma with $n<n_c/4$ is given by $I_R=I_n\exp(G_0LI)$, where $G_0=1.59\times10^{-13}$ cm/W for a 1054-nm laser and $n=0.1n_c$, and I_n is the noise level from which the Raman instability grows.[1,15] If one uses the time-averaged intensity of the ISI beam, the above formula predicts much less Raman gain than is experimentally observed with the combination of the ISI beam and a preplasma target.

The following modification to the theory provides better agreement with the experiment. The homogeneous plasma growth rate[1,15] for Raman backscattering with $n=0.1n_c$ is larger than the laser bandwidth $\Delta\omega=2\pi/\tau_c=3\times10^{12}$ sec^{-1} for intensities above 5×10^{13} W/cm^2. The instabililty should therefore respond to the instantaneous intensity peaks in the focal distribution with ISI. We therefore modified the usual theory for Raman gain with the assumption that the instability grows convectively to saturation in these instantaneous hot spots. The instantaneous intensity distribution at the target with ISI is accurately approximated by the probability distribution, $P(I)=(1/I_0)\exp(-I/I_0)$, provided that the intensity is not modified by filamentation. Integrating the Raman gain over $P(I)$, one obtains the following expression for the Raman backscatter I_R:

$$I_R=I_n\int_0^{I_s}P(I)e^{G_0LI}dI+\alpha\int_{I_s}^{\infty}IP(I)\,dI\,. \tag{1}$$

Here I_s is the incident intensity which satisfies $\alpha I_s=I_n\exp(G_0LI_s)$, where α is a saturated-reflectivity coefficient.

The solid curve in Fig. 3 shows the best fit of Eq. (1) to the preplasma data using L and α as free parameters. I_n was estimated to be the emission from a blackbody source (1.7 kW/sr cm^2 nm) with the coronal plasma temperature ($T_e=1200$ eV from computer simulations) integrated over the solid angle (0.008 sr) of the focusing lens. A constant I_{pp} was added to the Raman intensity calculated by Eq. (1) to match the emission observed from the preplasma alone ($I_T=I_R+I_{pp}$). Equation (1) was also integrated over the sinc^2 spatial intensity distribution obtained with ISI. The best fit occurs for $L=0.09$ cm and $\alpha=5\times10^{-6}$ nm^{-1}; this α limits the backscatter through the lens to 0.0005% of the incident intensity per nm of Raman wavelength. The dashed curve in Fig. 3 corresponds to the average $L=0.065$ cm obtained from the hydrocode, but uses the same α. An increase or decrease in α by several orders of magnitude does not have a significant effect on the theoretical intensity threshold at which the backscatter first emerges above the background emission; thus it is not necessary to know α precisely to predict the onset of Raman backscatter with Eq. (1). The small Raman emission that is observed at the highest intensities with ISI, but without the preplasma, can be fitted to the predictions of Eq. (1) using a shorter density scale length, $L=0.05$ cm.

The curves in Fig. 3 indicate that the onset of Raman backscatter occurred in our experiment with a LI_0G_0 product that is 30% lower than that predicted by Eq. (1). This disagreement between theory and experiment may reflect several factors. First, since a variation of L in Eq. (1) is mathematically equivalent to the same percentage variation in G_0, the discrepancy could be accounted for by a small (30%) error in the theoretical G_0. Second, the experimental I_0 and the density scale length L are known to an absolute accuracy of only $\pm15\%$. Third, Eq. (1) does not account for all physics effects. For example, simulations indicate that the instantaneous intensity structure with broadband ISI can suffer a weak ponderomotive filamentation with our experimental conditions.[12] This would place somewhat more energy at higher intensity than $\exp(-I/I_0)$, and thereby the Raman gain could increase.

In experiments without ISI, a gap has often been observed in the Raman spectrum between $2\lambda_0$ and the scattering observed at shorter wavelengths. It has been proposed that SBS causes a localized disruption of the Raman instability and thereby produces the spectral gap.[13] Paradoxically, there could be more Raman backscatter with broadband ISI in the "spectral gap" region due to suppression of Brillouin scattering. A comparison of the backscatter results with the preplasma at two different wavelengths indicates that this phenomenon may be occurring. With broadband ISI the $1.73\lambda_0$ backscatter at an 8° angle had similar threshold and growth with laser intensity as the results shown for $1.53\lambda_0$ in Fig. 3. With narrow-band ISI, the backscatter at $1.73\lambda_0$ was less than that obtained with broadband ISI. In contrast, at $1.53\lambda_0$ the threshold energy for appreciable backscatter was much lower and the backscatter amplitudes much higher with narrow-band ISI than with broadband ISI. Copious SBS was observed with narrow-band ISI.[14] Despite its suppression of SBS, broadband ISI had a net beneficial effect in reducing Raman backscatter. The net, spectrally integrated backscatter over the range $(2.1-1.3)\lambda_0$ at angles of 0° and 8° was found to be much smaller ($>10\times$ reductions) with broadband ISI than with either narrow-band ISI or the ordinary beam for all the experimental conditions studied here.

In summary, this experiment indicates that the onset of Raman scattering produced with an ISI-smoothed laser beam can be predicted rather well by a convective model that accounts for the instantaneous focal pattern. Additional suppression of Raman backscatter by ISI may be available at larger bandwidths than used here so that $\Delta\omega$ becomes larger than the Raman growth rates.

We wish to acknowledge useful discussions with R. H. Lehmberg, K. Kearney, J. Grun, M. Pronko, and C. K. Manka. The technical assistance of N. E. Nocerino, L. Daniels, J. Ford, and J. Bone is gratefully acknowledged. This work was supported by the U.S. Department of Energy.

[1]C. S. Liu, M. N. Rosenbluth, and R. B. White, Phys. Fluids **17**, 1211 (1974).

[2]K. Tanaka *et al.*, Phys. Rev. Lett. **48**, 1179 (1982).

[3]C. L. Shepard *et al.*, Phys. Fluids **29**, 583 (1986).

[4]W. K. Seka *et al.*, Phys. Fluids **27**, 2181 (1984).

[5]R. P. Drake *et al.*, Phys. Rev. Lett. **60**, 1018 (1988).

[6]R. E. Turner *et al.*, Phys. Rev. Lett. **54**, 189 (1985); R. P. Drake *et al.*, in Proceedings of the Eighteenth Conference on Anomalous Absorption, Quebec, 1988 (to be published).

[7]D. W. Phillion *et al.*, Phys. Fluids **25**, 1434 (1982).

[8]H. C. Barr *et al.*, Phys. Rev. Lett. **60**, 1950 (1988).

[9]Albert Simon and Robert W. Short, Phys. Rev. Lett. **53**, 1912 (1984).

[10]R. H. Lehmberg and S. P. Obenschain, Opt. Commun. **46**, 27 (1983).

[11]S. P. Obenschain *et al.*, Phys. Rev. Lett. **56**, 2807 (1986).

[12]A. J. Schmitt, Phys. Fluids **31**, 3079 (1988).

[13]D. M. Villeneuve *et al.*, Phys. Rev. Lett. **59**, 1585 (1987).

[14]A. N. Mostovych *et al.*, Phys. Rev. Lett. **59**, 1193 (1987).

[15]Kent Estabrook and W. L. Kruer, Phys. Rev. Lett. **53**, 465 (1984).